Development and application of automated vicarious calibration system

Wei Wei (韦 玮)[1,2], Shuai Song (宋 帅)[3], Yangang Sun (孙彦港)[4], Ganggang Qiu (邱刚刚)[1,2], Xin Li (李 新)[1], and Xiaobing Zheng (郑小兵)[1,*]

[1]*Key Laboratory of Optical Calibration and Characterization, Anhui Institute of Optics and Fine Mechanics, Chinese Academy of Sciences, Hefei 230031, China*

[2]*University of Sciences and Technology of China, Hefei 230026, China*

[3]*Troop 61741 of PLA, Beijing 100094, China*

[4]*Shanghai Maritime University, Shanghai 201306, China*

**Corresponding author: xbzheng@aiofm.ac.cn*

Received April 7, 2017; accepted July 5, 2017; posted online July 26, 2017

In order to improve the frequency and precision of radiometric calibration, the automated vicarious calibration system (AVCS) is developed and deployed at the Dunhuang test site to perform vicarious calibration without the *in situ* manned measurements. The surface and atmospheric parameters are automatically collected by AVCS. An absolute radiometric calibration approach based on AVCS is proposed. Six successful calibrations of the Aqua Moderate Resolution Imaging Spectroradiometer (MODIS) are conducted. The results are in good agreement with the on-board calibration system with all the relative differences less than 4%. It enables us to monitor the change of a sensor over long time scales.

OCIS codes: 010.0280, 280.4788, 120.0280, 120.5630.
doi: 10.3788/COL201715.100101.

A key component to long time scales Earth observation is the radiometric calibration of the remote sensing sensor used to view the earth[1,2]. The physical interpretation of remote sensing data and the change monitoring of the sensor both require an accurate radiometric calibration[3]. The vicarious calibration (VC), the process of converting on-board sensor output digital numbers (DNs) to spectral radiance in place of laboratory calibration and on-board calibration, is a mature and reliable method for post-launch calibration[1,4,5]. It helps us to understand whether changes collected in the data are due to the sensor or the actual scene because of its independence from the sensor and any on-board calibration system[6].

Traditional VC relies on measurements of the surface and atmospheric properties of the calibration test site at the moment of satellite overpass. These data of *in situ* measurements, including surface reflectance, aerosol optical depth (AOD), column ozone amount, and column water vapor amount, in conjunction with satellite geometry and solar geometry, are input into the radiative transfer model (RTM) to predict the top-of-atmosphere (TOA) band-averaged radiance of the sensor under test[7–9]. VC was recommended as the preferred method to calibrate the on-board sensor by a panel of calibration scientists at the October 2004 Committee on Earth Observations Satellites Optical/Visible working group meeting[10].

However, a drawback of traditional VC is the requirement of manned field campaign, which is labor-intensive and costly with the limitation of low frequency of data collections[11–13]. At present, only one calibration field campaign was conducted at the Dunhuang test site every year for a sensor. Nevertheless, this calibration frequency is insufficient to monitor the degradation of a sensor. The automated VC system (AVCS) that consists of three automated instruments and a data center was developed by the Anhui Institute of Optics and Fine Mechanics (AIOFM), Chinese Academy of Sciences (CAS) to increase the calibration frequency without the personnel presence[13–15]. It is a system that is capable of automatically collecting data that are needed to report the TOA spectral radiance and hope to retain the accuracy and precision consistent with the traditional approach. The three automated instruments were deployed at the Dunhuang test site, and the data center was in the Optical Remote Sensing Center, AIOFM. In this Letter, an absolute radiometric calibration approach based on AVCS was proposed. Six successful calibrations of the Aqua Moderate Resolution Imaging Spectroradiometer (MODIS) were conducted in 2 months.

The Dunhuang test site, one of the Chinese Radiometric Calibration Sites (CRCS) in Gobi desert, covers a relatively flat area of 25 km × 25 km. Its central region of 10 km × 10 km has a nice spatial heterogeneity of less than 2%[16], and it was selected as a standard reference site for the post-launch calibration of the spacecraft optical sensors by the Committee on Earth Observation Satellites[17]. A study on the temporal stability of surface reflectance of the Dunhuang test site was performed by analyzing the MODIS bidirectional reflectance distribution function (BRDF) products. The MODIS band nadir reflectance of the Dunhuang test site with same solar zenith of 63° was calculated to assess the temporal stability. As is shown in Fig. 1, the band nadir reflectance has a seasonal variation from 2008 to 2016. The relative

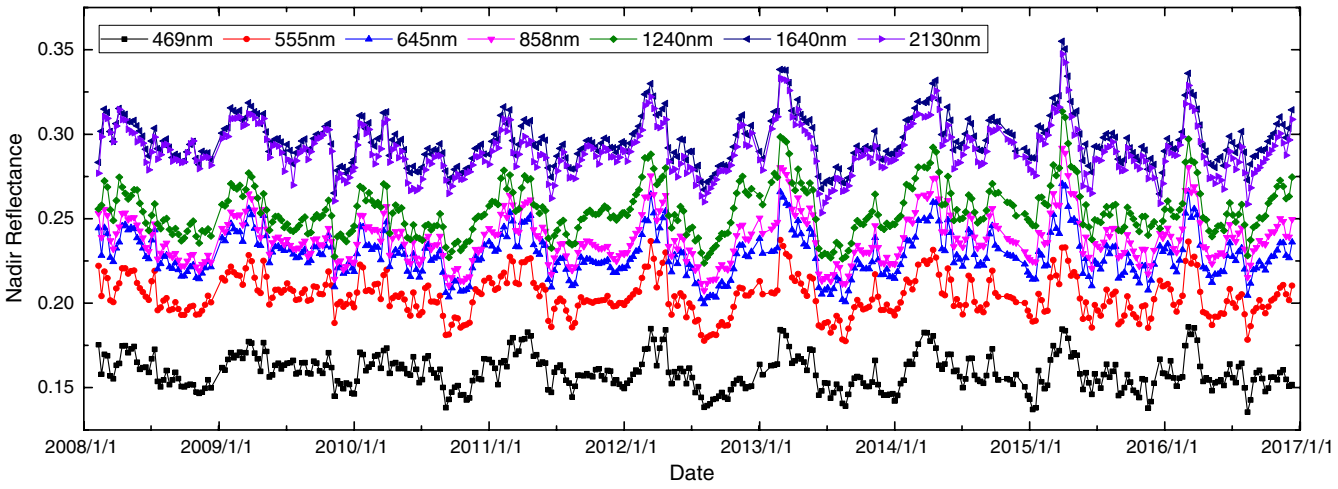

Fig. 1. (Color online) MODIS band reflectance of the Dunhuang test site from 2008 to 2016.

difference between annual maximum and annual minimum during a year is within 10.6%–27.1% in the past 9 years. It is unreasonable to use a time-invariant reflectance to describe the surface property of the Dunhuang test site throughout the year.

The three instruments of AVCS deployed in the Dunhuang test site to collect site parameters are the automated test-site radiometer (ATR), automated precision solar radiometer (PSR), and automated hyperspectral irradiance meter (HSIM), respectively. The data center is used to receive the field observation data by the BeiDou Navigation Satellite System (BDS) and the internet. The structure diagram of AVCS is shown in Fig. 2.

The ATR is an eight-band surface observation radiometer covering the wavelength range from 400 to 1600 nm, using interference filters coupled with silicon and InGaAs detectors. It samples surface radiance every 3 min with a 10° field of view (FOV). A TE cooler is used to control the optical head temperature to eliminate the influence of temperature. The ATR is powered by a solar power system and transmits data through the BDS[18–20]. The PSR is an eight-band sun photometer measuring the direct solar irradiance in the spectral range of 360–1040 nm. Its optical header is also temperature controlled; the same as the ATR. The data transmitting system is the BDS. A quadrant detector is used to automatically track the sun. AOD

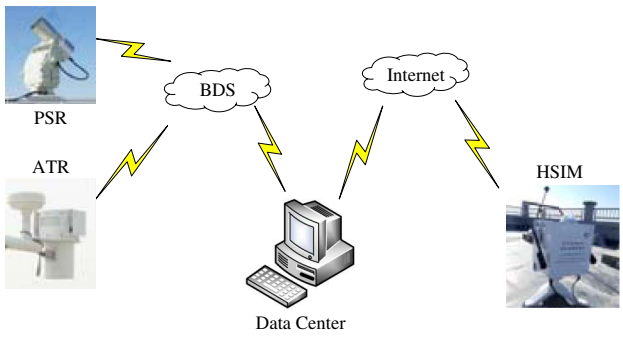

Fig. 2. Structure diagram of AVCS.

can be determined by a retrieval algorithm with the PSR's data[21–23]. Due to the intolerable error of diffuse irradiance predicted by the RTM[24], HSIM is used to determine the diffuse irradiance by measuring the diffuse-to-global spectral irradiance ratio. A black ball is used to automatically block the direct beam when measuring the diffuse irradiance[16]. HSIM covers a wavelength range of 400–2400 nm. It sends data to the data center via the internet. The three instruments are all field hardened, weatherproof, and automated. This makes it possible to have long-term automatic observation without personnel. Figure 3 shows the three automatic instruments and the Dunhuang test site observation station. The spectral characteristics of the ATR and PSR are described in Table 1.

In our absolute radiometric calibration approach based on AVCS, the surface reflectance can be obtained without the need of a reference reflectance panel, using[8,25]

$$\rho_i = \frac{\pi C_i V_i}{E_i}, \tag{1}$$

Fig. 3. (a) ATR, (b) HSIM, (c) PSR, and (d) the Dunhuang test site observation station.

Table 1. Spectral Characteristics of ATR and PSR

	Center Wavelength (nm)	
Band	ATR	PSR
1	405	365
2	450	410
3	525	500
4	610	610
5	700	670
6	808	860
7	980	940
8	1540	1024

$$E_i = \frac{E_{i,\text{direct}} \cos\theta_s}{1-\alpha_i}, \tag{2}$$

$$\alpha_i = \frac{E_{i,\text{diffuse}}}{E_{i,\text{global}}}, \tag{3}$$

where i is the ATR band number, ρ_i is the band-averaged reflectance of the ATR, E_i is the ATR band-averaged global irradiance at the ground level, V_i is the output voltage of the ATR, C_i is the ATR calibration coefficient determined by laboratory calibration, $E_{i,\text{direct}}$ is the ATR band-averaged direct irradiance at the ground level computed using MODerate resolution atmospheric TRANsmission 4 (MODTRAN4), θ_s is the solar zenith angle, and α_i is the band-averaged diffuse-to-global ratio at the ground level. $E_{i,\text{diffuse}}$ is the ATR band-averaged diffuse irradiance measured by HSIM, and $E_{i,\text{global}}$ is the ATR band-averaged global irradiance measured by HSIM. The AOD needed for MODTRAN4 is retrieved from the PSR data. Figure 4 shows the ATR band-averaged reflectance obtained by AVCS.

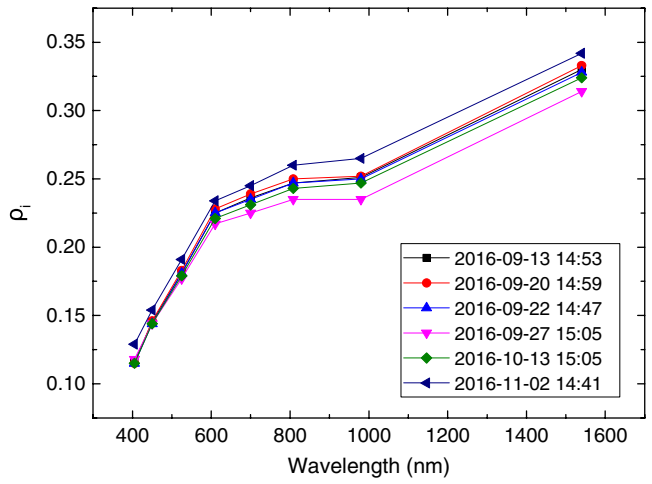

Fig. 4. (Color online) ATR band-averaged reflectance obtained by AVCS.

As a general calibration system, the desire to be able to calibrate any reflective solar band of a given sensor requires real-time hyperspectral reflectance of the test site surface. The ATR multispectral reflectance must be converted to hyperspectral reflectance. By analyzing the surface hyperspectral and multispectral reflectance of the Dunhuang test site, we found that the spectral reflectance of the Dunhuang test site has a stable spectrum shape, as is shown in Fig. 5. It means that we can get a real-time hyperspectral reflectance by scaling a reference hyperspectral reflectance with an adjustment of up and down. The scaling factor k is determined by calculating a weighted average of the samples for each ATR band to avoid gross error caused by an anomaly. It is chosen to minimize the value of W in the following[8]:

$$W = \sqrt{\sum_{i=1}^{8} \frac{1}{\sigma_i} [\rho_i - (k + \rho_{i,\text{ref}})]^2}, \tag{4}$$

where i is the ATR band number, ρ_i is the ATR band-averaged reflectance determined by AVCS, $\rho_{i,\text{ref}}$ is the ATR band-averaged reflectance computed from the reference hyperspectral reflectance, and σ_i is the standard deviation of the retrieved ρ_i. The scaling result is shown in Fig. 6.

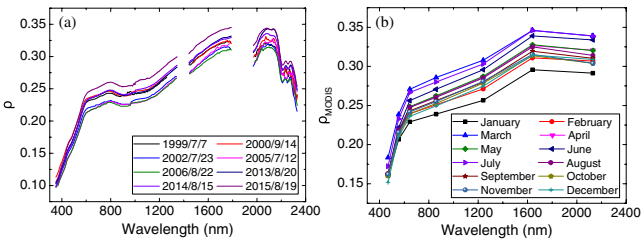

Fig. 5. (Color online) Spectral reflectance of the Dunhuang test site, (a) hyperspectral reflectance of *in situ* measurement and (b) monthly averaged MODIS band reflectance obtained from MODIS product, 2016.

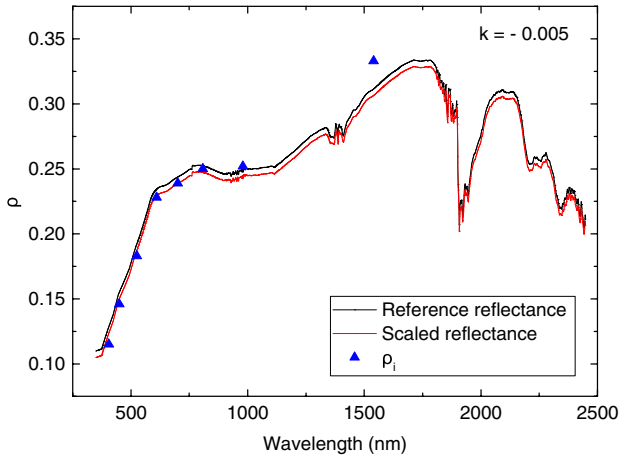

Fig. 6. (Color online) Scaling result of the Dunhuang test site on September 9, 2016.

Due to the non-Lambert characteristic of the Dunhuang test site, a BRDF model of the Dunhuang test site supported by National Satellite Meteorology Center, China Meteorological Administration was used to get the reflectance in the viewing direction. The BRDF model can be expressed as[17,26]

$$\rho_M(\theta_v,\theta_s,\varphi) = f_{\text{iso}} + f_{\text{vol}}k_{\text{vol}}(\theta_v,\theta_s,\varphi) + f_{\text{geo}}k_{\text{geo}}(\theta_v,\theta_s,\varphi), \tag{5}$$

$$\rho_v(\theta_v,\theta_s,\varphi) = \frac{\rho_M(\theta_v,\theta_s,\varphi)}{\rho_M(0,\theta_s,0)} \cdot \rho_{\text{AVCS}}. \tag{6}$$

where $\varphi = \varphi_v - \varphi_s$, θ_v, φ_v, θ_s, and φ_s are the viewing zenith, viewing azimuth, solar zenith, and solar azimuth, respectively. $\rho_M(\theta_v,\theta_s,\varphi)$ is the reflectance in the viewing direction calculated by the BRDF model with the solar angle of (θ_s,φ_s). $k_{\text{vol}}(\theta_v,\theta_s,\varphi)$ and $k_{\text{geo}}(\theta_v,\theta_s,\varphi)$. are, respectively, the volume scattering kernel and geometrical optics scattering kernel only related to the viewing geometry. f_{iso}, f_{vol}, and f_{geo} are the factors related to the kernels. $\rho_M(0,\theta_s,0)$ is the nadir reflectance calculated by the BRDF model. ρ_{AVCS} is the nadir reflectance determined by AVCS. $\rho_v(\theta_v,\theta_s,\varphi)$ is the reflectance in the viewing direction of (θ_v,φ_v).

The TOA radiance is reported by the RTM second simulation of the satellite signal in the solar spectrum (6S) with the reflectance of the viewing direction. The predicted TOA radiance is compared to the sensor DN to determine the absolute radiometric calibration coefficient. The coefficients of the MODIS solar reflective band is computed, using

$$A_i = L_i/\text{DN}_i, \tag{7}$$

where i is the band number, A_i is the band calibration coefficient, L_i is the band-averaged TOA radiance, and DN_i is the observation data of MODIS band i.

In the 2 months after the deployment of the AVCS at the Dunhuang test site, six successful collections with a viewing zenith of less than 30° and a clear sky were used to calibrate the Aqua MODIS. The parameters used for the calibration expected for the spectral reflectance are all listed in Table 2. The AOD is retrieved using the data collected by the PSR. The reflectance used in this work is determined by the AVCS. The ozone amount is obtained from ozone monitoring instrument (OMI) data. The water vapor amount is obtained from the website of the Department of Atmospheric Science, College of Engineering, University of Wyoming. All of these data are input into the 6S to report the spectral apparent radiance. In conjunction with the sensor data, the coefficient is determined. The results are compared with the on-board calibration coefficients. The processing diagram of the calibration based on the AVCS is shown in Fig. 7.

As is shown in Table 3, in the time span of 2 months, the coefficients of the calibration based on the AVCS and the on-board system are in good agreement with all of the relative differences of less than 4%. The mean values are less than 3.4%, and the standard deviations are less than 1.5%, which show a great stability of this method. The results demonstrate that the calibration based on the AVCS without *in situ* manned measurement is feasible, and the accuracy is on par with the traditional approach. The main aspect that affects the accuracy of the approach based on the AVCS is the retrieval of surface spectral reflectance. The first factor is the inhomogeneity of the Dunhuang test site. Only one ATR with a 10° FOV was deployed, and the small area that the ATR views may not represent the surface property of the whole test site. The second factor is the scaling method of the hyperspectral reflectance curve. The water vapor amount obtained from website is daily averaged, which if used for the RTM may not represent the real-time value. The calibration based on the AVCS is modeled on the reflectance-based method. The selection of the aerosol model also affects the accuracy of the calibration.

For the calibration based on the AVCS, the main sources of reflectance measurement uncertainty originate from the determination of the ATR reflectance, scaling hyperspectral reference reflectance, and the spatial

Table 2. Satellite, Atmospheric, and Solar Parameters for Six Aqua MODIS Overpasses at the Dunhuang Test Site

Date	2016/9/13	2016/9/20	2016/9/22	2016/9/27	2016/10/13	2016/11/2
Time(Beijing)	14:53	14:59	14:47	15:05	15:05	14:41
Viewing zenith	6.86	18.02	4.7	28.11	28.21	14.818
Viewing azimuth	257.3	261.28	74.96	261.35	261.19	75.747
Solar zenith	40.27	43.61	43.26	46.97	53.05	57.745
Solar azimuth	209.85	211.25	206.93	212.45	210.65	201.586
AOD550	0.112	0.276	0.216	0.336	0.169	0.147
O3 (DU)	278	277	284	272	290	282
Water vapor (g/cm^2)	0.992	1.272	1.093	1.239	0.359	0.539

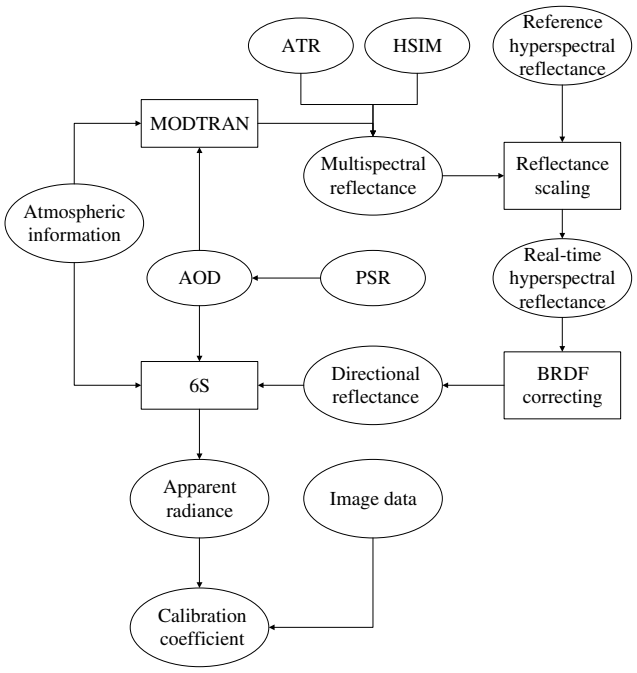

Fig. 7. Processing scheme of the calibration based on AVCS.

Table 4. Uncertainty Calibration Based on AVCS

Error Sources	Uncertainty (%)	Total Uncertainty (%)
Reflectance measurement		4.5
ATR reflectance	3.1	
Scaling reference data	2.6	
Spatial heterogeneity	2	
AOD		2.1
Aerosol model		1.7
RTM		1.0
NonLambert		1.5
Solar zenith angle		2.0
Water vapor		2.2
Total		6.3

heterogeneity of test site[26]. The respective uncertainties are 3.1%, 2.6%, and 2%, and the total uncertainty of reflectance measurement is 4.5%. The uncertainty of the ATR reflectance determination includes radiometric calibration of ATR, computation of the direct irradiance at ground level, and the measurement of the diffuse-to-global ratio. The error sources and corresponding uncertainties are summarized in Table 4[5,15,27,28].

The AVCS is developed and deployed at the Dunhuang test site. The main goal of the AVCS is to increase the temporal frequency of calibration without the *in situ* personnel and to keep the accuracy consistent with the manned VC. Six successful calibrations of the Aqua MODIS are conducted based on the AVCS in 2 months. The results are encouraging and show a good agreement with the on-board calibration results. The deployment of the AVCS makes it possible to monitor the change of the sensor with a high temporal frequency over the long time scales. There are still some inconsistencies in the results, and this can be attributed to the retrieval of the surface spectral reflectance. Future work should be focused on the solution to reduce the impact of the surface inhomogeneity and accuracy of the reference hyperspectral reflectance scaling.

This work was supported by the National Natural Science Foundation of China (No. 61505222), the Civil Aerospace Technology Advance Research Project (No. D040401), the United Foundation of Chinese Academy of Sciences (No. 6141A01011602), the Knowledge Innovation Program of the Chinese Academy of Sciences (No. CXJJ-15S103), and the Natural Science Foundation of Anhui Province (No. 1508085QD80).

Table 3. Relative Differences in Coefficient Between Calibration Based on AVCS and On-board System

	Relative Difference (%)							
MODIS Band	2016/9/13	2016/9/20	2016/9/22	2016/9/27	2016/10/13	2016/11/2	Mean	Standard Deviation
1	−0.71	0.94	−1.51	0.86	1.46	−1.00	0.01	1.23
2	1.78	2.75	0.96	1.40	0.56	0.12	1.26	0.97
3	−1.20	1.16	−1.38	−0.11	1.90	−1.53	−0.19	1.45
4	−1.02	0.39	−2.29	−0.19	0.74	−2.08	−0.74	1.27
5	0.68	2.45	0.59	1.21	1.39	0.97	1.21	0.68
6	1.79	3.61	2.86	3.13	2.91	3.94	3.04	0.74
7	−0.06	2.12	0.93	2.11	2.40	2.55	1.68	1.03

References

1. K. J. Thome, Remote Sens. Environ. **78**, 27 (2001).
2. J. S. Czapla-Myers, K. J. Thome, and N. P. Leisso, Proc. SPIE **6684**, 668407 (2007).
3. A. Meygert, R. Santer, and B. Berthelot, Proc. SPIE **8153**, 815311 (2011).
4. P. N. Slater, S. F. Biggar, K. J. Thome, D. I. Gellman, and P. R. Spyak, J. Atmos. Oceanic Technol. **13**, 349 (1996).
5. S. F. Biggar, "In-flight methods for satellite sensor absolute radiometric calibration," Ph.D thesis (University of Arizona, 1990).
6. J. S. Czapla-Myers, K. J. Thome, B. R. Cocilovo, J. T. McCorkel, and J. H. Buchanan, Proc. SPIE **7081**, 70810I (2008).
7. M. Dinguirard and P. N. Slater, Remote Sens. Environ. **68**, 194 (1999).
8. J. S. Czapla-Myers, "Automated ground-based methodology in support of vicarious calibration," Ph.D. thesis (University of Arizona, 2006).
9. J. S. Czapla-Myers and N. P. Leisso, Proc. SPIE **7807**, 78070R (2010).
10. D. X. Kerola, C. J. Bruegge, H. N. Gross, and M. C. Helmlinger, IEEE Trans. Geosci. Remote Sens. **47**, 1244 (2009).
11. N. J. Anderson and J. S. Czapla-Myers, Proc. SPIE **8866**, 88660N (2010).
12. K. J. Thome, J. S. Czapla-Myers, N. P. Leisso, J. T. McCorkel, and J. H. Buchanan, in *Proceedings of IEEE International Geoscience and Remote Sensing Symposium* (2008), p. 1332.
13. X. Li, Y. Yin, E. Liu, Y. Zhang, L. Xun, W. Wei, Z. Zhang, G. Qiu, Q. Zhang, and X. Zheng, Proc. SPIE **9264**, 92640V (2014).
14. X. B. Zheng, J. Atmos. Environ. Opt. **9**, 2 (2014).
15. G. Qiu, X. Li, X. Zheng, J. Yan, and Y. Sun, Chin. Opt. Lett. **14**, 121201 (2016).
16. W. Wei, X. Li, C. Zhao, G. Qiu, and X. Zheng, Proc. SPIE **10156**, 101561M (2016).
17. Y. Li, Z. Rong, L. Zhang, L. Sun, and N. Xu, Proc. SPIE **9264**, 926415 (2014).
18. X. Li, X. B. Zheng, and Y. P. Yin, J. Atmos. Environ. Opt. **9**, 17 (2014).
19. Y. P. Yin, X. Li, X. B. Zheng, Z. P. Zhang, and W. Wei, J. Atmos. Environ. Opt. **11**, 44 (2016).
20. Y. P. Yin, "Development of automated site radiometer," Master thesis (University of Chinese Academy of Sciences, 2015).
21. G. Qiu, X. Li, X. Zheng, Q. Zhang, and J. Yan, Proc. SPIE **10155**, 101551R (2016).
22. M. Xia, J. Li, Z. Li, D. Gao, W. Pang, D. Li, and X. Zheng, Chin. Opt. Lett. **12**, 121201 (2014).
23. H. H. Asadov and I. G. Chobanzadeh, Chin. Opt. Lett. **7**, 760 (2009).
24. N. P. Leisso and J. S. Czapla-Myers, Proc. SPIE **8153**, 815210 (2011).
25. J. S. Czapla-Myers, N. P. Leisso, N. J. Anderson, and S. F. Biggar, Proc. SPIE **8390**, 83902B (2012).
26. Z. L. Liu, R. Chen, N. F. Liao, and Y. Wang, Chin. Opt. Lett. **10**, S11201 (2012).
27. J. Czapla-Myers, J. McCorkel, N. Anderson, K. Thome, S. Biggar, D. Helder, D. Aaron, L. Leigh, and N. Mishra, Remote Sens. **7**, 600 (2015).
28. S. Fan, M. Liu, and H. Shen, Chin. Opt. Lett. **12**, 051201 (2014).